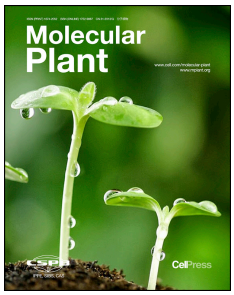
Journal Pre-proof



Dampened Nuclear Localization of SnRK1 by Brassinosteroid Signaling Inhibits Stomatal Development in Arabidopsis

Lianmei Yao, Shurui Liu, Wen Shi, Yuxin Gan, Min Fan, Filip Rolland, Ming-Yi Bai, Chao Han

PII: S1674-2052(25)00242-4

DOI: https://doi.org/10.1016/j.molp.2025.07.013

Reference: MOLP 1950

To appear in: *MOLECULAR PLANT*

Received Date: 2 February 2025

Revised Date: 17 June 2025

Accepted Date: 18 July 2025

Please cite this article as: Yao L., Liu S., Shi W., Gan Y., Fan M., Rolland F., Bai M.-Y., and Han C. (2025). Dampened Nuclear Localization of SnRK1 by Brassinosteroid Signaling Inhibits Stomatal Development in Arabidopsis. doi: https://doi.org/10.1016/j.molp.2025.07.013.

This is a PDF file of an article that has undergone enhancements after acceptance, such as the addition of a cover page and metadata, and formatting for readability, but it is not yet the definitive version of record. This version will undergo additional copyediting, typesetting and review before it is published in its final form, but we are providing this version to give early visibility of the article. Please note that, during the production process, errors may be discovered which could affect the content, and all legal disclaimers that apply to the journal pertain.

© 2025 CAS Center for Excellence in Molecular Plant Sciences, Chinese Academy of Sciences, and Chinese Society for Plant Biology. Published by Elsevier Inc. All rights are reserved, including those for text and data mining, AI training, and similar technologies.

Title: Dampened Nuclear Localization of SnRK1 by Brassinosteroid Signaling Inhibits Stomatal Development in Arabidopsis

Lianmei Yao[1], Shurui Liu[1], Wen Shi[1], Yuxin Gan[1], Min Fan[1], Filip Rolland[2], Ming-Yi Bai[1]* and Chao Han[1]*

[1]The Key Laboratory of Plant Development and Environmental Adaptation Biology, Ministry of Education; Shandong Key Laboratory of Precision Molecular Crop Design and Breeding; School of Life Sciences, Shandong University, Qingdao 266237, China.

[2] Laboratory for Plant Metabolic Signaling, Biology Department, KU Leuven, and KU Leuven Plant Institute (LPI), Kasteelpark Arenberg 31, 3001 Heverlee, Leuven, Belgium.

*Address correspondence to Chao Han (hanchao@sdu.edu.cn) and Ming-Yi Bai (baimingyi@sdu.edu.cn). The author responsible for distribution of materials integral to the findings presented in this article in accordance with the policy described in the Instructions for Authors is: Chao Han (hanchao@sdu.edu.cn) and Ming-Yi Bai (baimingyi@sdu.edu.cn).

Short Summary: The fate of meristemoids in leaf epidermis determinates the density and pattern of stomata, which is the channel to atmosphere and facilitates carbon acquirement for plants. The nuclear localization of KIN10, catalytic subunit of SnRK1, is critical for meristemoids transferring to stomata. Brassinosteroid signaling inhibits KIN10 nuclear localization via BIN2 mediated phosphorylation on KINβ2, which enhances KIN10-KINβ2 interaction and maintains KINβ2 membrane association.

Journal Pre-proof

Abstract: The balance between stem cell division and differentiation is crucial for flexible organ development. In Arabidopsis leaves, the fate of meristemoids, which exhibit stem cell characteristics, is tightly regulated by multiple intrinsic developmental signals and environmental factors. KIN10, catalytic subunit of Sucrose Non-Fermenting 1 (SNF1) related protein kinase 1 (SnRK1) complex, has been shown to preferentially localize in the nucleus of meristemoids, where it phosphorylates and stabilizes SPEECHLESS transcription factor, thereby promoting stomatal development. However, the regulatory mechanism governing the nuclear localization of KIN10 in meristemoids remains unclear. Here, we demonstrate that brassinosteroid (BR) inhibits KIN10's nuclear localization by modulating KINβ2 through BIN2-mediated phosphorylation. In meristemoids, KIN10 is predominantly nuclear, while KINβ2 is mainly cytosolic. Interfering nuclear localization of KIN10 or enhancing membrane association of KINβ2 impairs stomatal development and leads to excessive epidermal cell proliferation. BR signaling could inhibit KIN10 nuclear localization through enhancing KINβ2 membrane association. BR-INSENSITIVE2 (BIN2) interacts with and phosphorylates KINβ2, which reduces its membrane association and its interaction with KIN10. These findings suggested the precise regulation of subcellular localization of SnRK1 complex, influenced by BR signaling, is critical for meristemoids differentiation and stomatal development.

Key words: SnRK1, BIN2, Brassinosteroid, Stomatal development

Journal Pre-proof

Introduction

Stem cells exhibit self-renew and produce progeny that subsequently differentiate into specific cell types, which is essential for multicellular plants to continuously and flexibly build tissues and organs (Rasmussen et al., 2011; Heidstra and Sabatini, 2014). In the leaf epidermis, stomatal pores, made up by a pair of specialized guard cells, play vital roles in regulating gaseous exchange between the internal leaf air spaces and the atmosphere (Lawson and Matthews, 2020; Lawson and Blatt, 2014). Stomatal development initiates from meristemoid mother cells (MMCs), which acquire stem cell characteristics and undergo several times of asymmetric divisions to generate more meristemoids (M) and larger stomatal lineage ground cells (SLGCs) before terminal differentiation into guard mother cells (forming stomata by symmetrical division) or pavement cells, respectively (Bergmann and Sack, 2007; Pillitteri and Torii, 2012).The division and differentiation of M cells are tightly controlled by the closely related and sequentially expressed basic helix-loop-helix (bHLH) transcription factors SPEECHLESS (SPCH) and MUTE (Pillitteri et al., 2007; MacAlister et al., 2007). SPCH is responsible for initiating the stomatal lineage and continued proliferation of both M and SLGCs (Pillitteri et al., 2007). MUTE is a direct target of SPCH and is activated after one or several rounds of asymmetric divisions to trigger differentiation (Lau et al., 2014; Han et al., 2018).

The plasticity of stomatal development is regulated by hormonal, nutrient, and environmental factors (Qi and Torii, 2018; Zhang et al., 2023; Wang et al., 2024). Brassinosteroids (BR) are a group of plant steroid hormones that play critical roles in plant development. BR signaling initiates when the BRASSINOSTEROID INSENSITIVE 1 (BRI1) receptor kinase binds to brassinosteroids (BR), leading to the inhibition of the GSK3-like kinase BRASSINOSTEROID INSENSITIVE 2 (BIN2) through a phosphorylation cascade, which subsequently activates the transcription factors BRASSINAZOLE-RESISTANT 1 (BZR1) and BRI1-EMSSUPPRESSOR1 (BES1) to regulate the expression of BR target genes (Nolan et al., 2020; Kim and Wang, 2010; Han et al., 2023). Both BR biosynthesis and BR signaling mutants exhibit excess

stomata, indicating the essential role of BR in stomatal development (Kim et al., 2012). In M cells, the polarized scaffolding protein POLAR together with BREAKING OF ASYMMETRY IN THE STOMATAL LINEAGE (BASL) recruits BIN2 in plasma membrane to phosphorylate and inhibit MAPK kinase kinase (MAPKKK) YDA, the negative regulator of SPCH, to enhance M cell division and differentiation by maintaining SPCH stability (Houbaert et al., 2018). In contrast, the polarized protein phosphatase BSL1 interacts with BIN2 and promotes BIN2 partitioning to the nucleus in SLGCs through releasing the interaction and polarization of BIN2 and BASL (Guo et al., 2021). In SLGCs, BIN2 also interacts with and phosphorylates SPCH directly in the nucleus to turn it unstable, subsequently leading SLGCs to form pavement cells (Gudesblat et al., 2012).

Sucrose Non-Fermenting 1 (SNF1) related protein kinase 1 (SnRK1) is a conserved energy homeostasis regulator in plant cells, orthologous to the AMP-ACTIVATED KINASE (AMPK) in mammals and SNF1 in yeast, respectively (Li et al., 2021; Han et al., 2024). SnRK1 is a heterotrimeric complex, including a catalytic α subunits (KIN10 and KIN11), a regulatory β subunits (KINβ1, KINβ2, or the plant-specific truncated KINβ3), and a plant-specific hybrid γ subunit (KINβγ) (Broeckx et al., 2016; Van Leene et al., 2022). The β subunits of SnRK1 possess myristoylation modification and membrane associated localization, which can restrict KIN10 localizing in cytoplasm (Ramon et al., 2019). Energy stress, for example caused by darkness or hypoxia, promotes KIN10 nuclear translocation and transcriptional reprogramming of amino acid and mitochondrial respiratory metabolism through phosphorylating C type bZIP transcription factors (Ramon et al., 2019; Pedrotti et al., 2018; Mair et al., 2015). Meanwhile, KIN10 exhibits a predominantly nuclear localization in the root meristematic zone, which is repressed by abscisic acid (ABA) signaling for stress-induced cytosolic KIN10-mediated root growth arrest (Belda-Palazón et al., 2022). Besides, the specific nuclear localization of KIN10 also exhibits in M cells and guard cells of leaf epidermis (Han et al., 2020). In M cells, KIN10 phosphorylates and stabilizes SPCH to promote stomatal development, which is also

important for stomatal density regulation by photosynthesis driving sucrose production (Han et al., 2020). In guard cells, KIN10 phosphorylates bZIP30 transcriptional factor, promoting its interaction with BZR1, which in turn induces guard cell starch degradation and promotes light-induced stomatal opening (Shi et al., 2024). Hydrogen peroxide (H_2O_2) accumulates in a cell-type-specific manner in both M cells and guard cells, where it represses the interaction between KINβ2 and KIN10, leading to the nuclear localization of KIN10 in these cell types. This process promotes stomatal development in M cells and stomatal opening in guard cells, respectively (Shi et al., 2022).

Our previous study showed that KIN10 preferentially localizes in the nucleus of M cells, where it phosphorylates SPCH to enhance its protein stability and promote stomatal development (Han et al., 2020). However, the regulatory mechanism governing the nuclear localization of KIN10 in M cells remains unclear. Here, we demonstrate that BR inhibits nuclear localization of KIN10 by modulating KINβ2 through BIN2-mediated phosphorylation. We show that the nuclear localization of KIN10 and the plasma membrane-dissociation of KINβ2 are required for the differentiation of M cell into stomatal guard cells. BR promotes plasma membrane association of KINβ2 and reduces the nuclear localization of KIN10. BIN2 directly interacts with and phosphorylates KINβ2, inhibiting its interaction with KIN10 and results in KIN10 nuclear localization in M cells. These findings provide valuable insights into the precise regulation mechanism by which BR regulates the subcellular localization of the SnRK1 complex, a process crucial for M cell fate determination and stomatal development.

Results:

Nuclear-localized KIN10 is required for meristemoid differentiation

In Arabidopsis, MMCs acquire stem cell characteristics and undergo asymmetric division, which generates a smaller M cell and a larger SLGC. Our previous study showed that KIN10 promotes stomatal development by phosphorylating and stabilizing

SPCH (Belda-Palazón et al., 2022). We also observed that KIN10 is predominantly localized in the nucleus of M cells but exhibits weak nuclear localization in SLGCs (Figure 1A and 1B). This differential localization suggests that nuclear localization of KIN10 may be crucial for M cell fate determination. To test this hypothesis, we used transgenic plants in the *kin10kin11* double mutant background, expressing a flag-tagged wild-type KIN10, a nuclear localized form of KIN10 (fused with the SV40 nuclear localization sequence (Adam et al., 1989), nlsKIN10), or a membrane-associated version of KIN10 (fused with the KINβ2 subunit an N-terminal myristoylation motif, myrKIN10) under *KIN10* native promoter control (Ramon et al., 2019). Both the *kin10* mutant, *kin11* mutant (mutation of functionally redundant catalytic subunits of SnRK1 complex) and the *kin10*$^{-/-}$ *kin11*$^{+/-}$ loss-of-function sesqui-mutant exhibited a reduced stomatal index, which is the number of stomata relative to the total number of epidermal cells (Figure 1 C and Figure S1). Complementation of *kin10kin11* double mutant with the wild-type *KIN10* and *nlsKIN10* restored the stomatal index and leaf epidermal cell pattern to levels similar to those of wild-type plants. However, complementation of *kin10kin11* double mutant with the membrane-associated *myrKIN10* in *kin10kin11* double mutant background did not rescue stomatal development and resulted in a stomatal index comparable to that of the *kin10*$^{-/-}$ *kin11*$^{+/-}$ mutant (Figure 1C and 1D). The *kin10*$^{-/-}$ *kin11*$^{+/-}$ mutant generated more epidermal cells than the wild-type. And epidermal cell density was also much higher in the *myrKIN10-flag kin10 kin11* line than in the *nlsKIN10-flag kin10 kin11* and *KIN10-flag kin10 kin11* lines (Figure 1C and 1E). This genetic evidence suggested that the nuclear-localized KIN10 is required for stomatal development.

To further confirm the function of nuclear-localized KIN10 in M cell fate determination, we examined the number of cells surrounding stomata. In Arabidopsis leaves, stomata often exhibit anisocytic complexes, where each stoma is surrounded by varying numbers or monoclonal SLGCs due to the additional amplifying divisions of M cells (Nadeau and Sack, 2002). In wild-type plants, approximately 60% of stomata associated with a single cell after a minimal spacing division. In contrast, the *kin10* and

kin10$^{-/-}$ *kin11*$^{+/-}$ mutants showed a higher proportion of anisocytic complexes, with more than four surrounding cells. Complementation of the *kin10 kin11* double mutant background with wild-type *KIN10* restored the proportion of one-cell-separated stomata and the distribution of anisocytic complexes to wild-type plant levels. Similarly, complementation with nlsKIN10 increased the number of one-cell-separated stomata, while complementation with myrKIN10 resulted in similar numbers of one-cell-separated stomata and anisocytic complexes as in the *kin10*$^{-/-}$ *kin11*$^{+/-}$ mutant (Figure S2). These findings suggested that nuclear-localized KIN10 promotes M cell differentiation by limiting excessive asymmetric divisions in M cells.

Previous study has shown that nuclear localization of KIN10 is involved in nitrate-induced lateral root elongation (Wang et al., 2022). To further investigate whether nuclear localization can fully rescue the phenotypes of *kin10* mutant, we examined the nitrate-promoted plant development in wild-type *KIN10*, *nlsKIN10* and *myrKIN10* transgenic lines. The results revealed that KIN10-flag, myrKIN10-flag, and nlsKIN10-flag lines all successfully rescued the longer lateral root of *kin10* mutant. Interestingly, nlsKIN10 exhibits a stronger inhibitory effect on lateral root elongation compared to wild-type KIN10, while myrKIN10 showed a weaker suppression effect than wild-type KIN10 (Figure S3). These findings indicate that both cytoplasmic-localized and nuclear-localized KIN10 play critical regulatory roles in KIN10-mediated root development processes, with nuclear-localized KIN10 having a significantly more pronounced inhibitory effect on lateral root elongation.

Plasma membrane-dissociated KINβ2 in meristemoid cells is crucial for stomatal development

Given the important role of KIN10 nuclear localization in M cell differentiation and the regulatory effect of KINβ subunits on localization of KIN10 (Van Leene et al., 2022), we investigated how the KINβ subunits influence M-cell differentiation. Arabidopsis encodes three KINβ subunits. To identify which KINβ subunit plays important roles for stomatal development, we examined the stomatal phenotypes of various *kinβ* mutants. Mutants with T-DNA insertions in *KINβ2* (*kinβ2-1* and *kinβ2-2*) exhibited an increased

193 stomatal index without altering the total cell number, suggesting that *KINβ2* mutation
194 enhances stomatal formation. Conversely, the *kinβ1-2* mutant displayed a reduced total
195 cell number but a similar stomatal index to wild-type plants. The *kinβ1-2 kinβ2-1* and
196 *kinβ1-2 kinβ2-2* double mutants exhibited both a reduced total cell number and
197 increased stomatal index. Mutation of *KINβ3,* encoding a truncated β subunit that lacks
198 the N-terminal MYR motif, resulted in an increased total cell number and a decreased
199 stomatal index, suggesting a different function compared to KINβ1 and KINβ2. The
200 triple mutant *kinβ-t* (*kinβ1-2 kinβ2-2 kinβ3*) exhibited fewer stomata and total cell,
201 along with the stomatal index, identifying KINβ2 as negative regulator for stomata
202 differentiation (Figure S4).

203 We then focused on *KINβ2* and analyzed its expression pattern in epidermal cells
204 by generating *pKINβ2::KINβ2-YFP* transgenic lines. Like *KIN10*, *KINβ2* is expressed
205 in all epidermal cells, but its subcellular localization varies depending on the cell type.
206 We analyzed the intracellular fluorescence intensity of KINβ2-YFP in different types
207 of cells and set Histone3-RFP as a reference protein for nucleus. In SLGC and pavement
208 cells, KINβ2 is mainly associated with the plasma membrane, while in most M cells
209 and guard cells, KINβ2 exhibits a cytosolic, diffused localization, indicating a partial
210 loss of plasma membrane anchoring ability in these cells (Figure 2A and 2B). To verify
211 the cell identity of cytosolic localization of KINβ2, we cross *pKINβ2::KINβ2-YFP* and
212 *pSPCH::SPCH-RFP* transgenic plants. The cytosolic and diffused localization of
213 KINβ2 is highly correct with SPCH-RFP expressed cells, confirming that KINβ2
214 exhibits a cytosolic, diffused localization in M cells (Figure S5A and S5B). Compared
215 to KIN10, which is predominantly localized in the nucleus of M cells and guard cells,
216 KINβ2 is found in the cytoplasm. However, in SLGC and pavement cells, KINβ2 and
217 KIN10 co-localize at the plasma membrane, consistent with KINβ2 facilitating the
218 plasma membrane localization of KIN10 (Figure 2A and 2B). To further confirm this
219 hypothesis, we detect the KIN10 localization in the *kinβ2* mutant background. Loss of
220 function of *KINβ2* results in clear nuclear localization of KIN10 in SLGC cells (Figure
221 2C and 2D).

To further confirm that the plasma membrane-dissociation of KINβ2 is critical for stomata development, we transformed wild-type KINβ2 and myrKINβ2 (which contains an additional myristoylation fused to KINβ2), both driven by the *SPCH* promoter, into the *kinβ2* mutant background. The myrKINβ2-RFP exhibited a much more tightly membrane-associated localization in M cells compared to KINβ2-RFP (Figure 2E). And co-transformation of myrKINβ2-YFP or KINβ2-YFP represses the nuclear localization of KIN10-RFP in tobacco leaves (Figure S6). Complementation with wild-type *KINβ2* restored the stomatal phenotype of *kinβ2* mutant to near wild-type. In contrast, complementation with *myrKINβ2* inhibited stomatal development, resulting in a reduced stomatal index and decreased stomatal density compared to wild-type plants (Figure 2F and 2G). Overall, these findings suggest that plasma membrane-dissociation of KINβ2 in M cells is crucial for KIN10 nuclear localization and stomatal development.

BR promotes the plasma membrane association of KINβ2

Previous studies have shown that BR signaling is attenuated in M cells [35]. Both BIN2 and BES1 are widely expressed in leaf epidermal cells but exhibit different localization patterns across leaf epidermal cell types. BIN2 is primarily associated with the plasma membrane in M cells, while BES1 is localized in the cytoplasm of M cells and the nucleus of SLGC and pavement cells (Houbaert et al., 2018; Kim et al., 2023). Given that KINβ2, like BIN2 and BES1, is broadly expressed in leaf epidermal cells but exhibits distinct localization patterns in M and SLGC cells, we hypothesize that BR signaling may influence the subcellular localization of KINβ2. To test this hypothesis, we firstly examined whether SnRK1 is involved in BR regulated stomatal development. The *bri1-116* is the BR insensitive mutant, while *bin2-1* is the BIN2 gain-of-function mutant (Peng et al., 2008; Wang et al., 2002). We crossed the *kin10* mutant with *bin2-1* and *bri1-116,* and then analyzed the stomatal development phenotypes of these lines. Quantitative RT-PCR analysis showed that the expression level of KIN10 and KINβ2 were similar in wild type, *bin2-1*, and *bri1-116* mutants (Figure S7A and S7B). The *kin10* mutant displayed a decreased stomatal index compared to wild-type plants, while

bin2-1 and *bri1-116* mutant exhibited an increased stomatal index and stomatal density. The *kin10 bin2-1* and *kin10 bri1-116* double mutant showed a stomatal index similar to those of the *kin10* mutant and less stomatal density compared with BR signaling deficit mutants. (Figure 3A-3C). We also crossed KINβ2 overexpression lines (*KINβ2-Ox*) with *bri1-116* mutant and analyzed the stomatal development phenotypes of these lines. Overexpression of *KINβ2* results in a decreased stomatal index and the stomatal density compared to wild-type plants, while the *bri1-116* mutant exhibited an increased stomatal index and stomatal density. The *KINβ2-Ox bri1-116* plants showed a stomatal index and stomatal density similar to those of *KINβ2-Ox* plants (Figure 3A, 3D and 3E). Besides, BR biosynthesis deficiency leads to higher stomatal index and the density of stomata caused by application of propiconazole (PPZ), a BRs biosynthesis inhibitor, which can be rescued by *KIN10* mutation and overexpression of *KINβ2* (Figure S8A-S8C). Together, these results suggested that SnRK1 complex function is involved in BR regulated stomatal development.

Next, we examined the localization of KINβ2 with and without BR treatment. We analyzed relative intracellular KINβ2 fluorescent intensity of M cells and SLGCs from more than 230 asymmetric divisions. Quantitative RT-PCR analysis showed that mutation of *BRI1* or *BIN2* did not have a significant effect on the expression of KINβ2-YFP (Figure S7C). In *bri1-116* and *bin2-1* mutant backgrounds, KINβ2 exhibited obviously increased intracellular fluorescence intensity in SLGC cells (Figure 4A and 4B). However, in the *bin2-1* mutant, intracellular fluorescent intensity of KINβ2 also exhibits slightly decreased in M cells compared to wild type plants (Figure 4B). Treatment with PPZ resulted in the dissociation of KINβ2 from the plasma membrane in SLGCs, but a slightly inhibited intracellular fluorescent intensity of KINβ2 in M cells. Importantly, membrane dissociation of KINβ2 in SLGCs was reversed by treatment with brassinolide (BL, the most active BR) or Bikinin, an inhibitor of GSK3 kinase (Figure 4C and 4D). And both BL and Bikinin treatment repress the intracellular fluorescent intensity of KINβ2 in M cells. These results suggest that BR signaling enhances the plasma membrane association of KINβ2.

BIN2 and BR signaling modulate KIN10 subcellular localization through the KINβ2 subunit

Given that KINβ2 modulates KIN10 subcellular localization and BR regulates the subcellular localization of KINβ2, we also examined KIN10 subcellular localization patterns in the epidermis in various BR signaling and biosynthesis-deficient mutant backgrounds. We crossed the *pKIN10::KIN10-YFP* line with *bri1-116*, *bin2-1* and *det2-1* mutants. In these mutants, we observed that a significant increase in the nuclear-to-cytoplasmic ratio of KIN10 in SLGCs compared to wild-type (Figure 4E and 4F). These results indicated that BR represses KIN10 nuclear localization.

In order to explore whether BR regulates KIN10 subcellular localization though the KINβ2 subunit, we examined the effects of BR on KIN10 subcellular localization in the leaf epidermal cells of wild type and *kinβ2* mutant plants. PPZ treatment promoted the nuclear localization of KIN10 in SLGCs, resulting in similar KIN10 nuclear/cytoplasmic ratio in M cells and SLGCs (Figure 4G and 4H). This increased nuclear localization of KIN10 in SLGCs was reversed by treatment of BL or Bikinin (Figure 4G and 4H). To further confirm these observations, we crossed *p35S::Histone3-RFP* with *pKIN10::KIN10-YFP*, using Histone3-RFP as a reference for nuclear localization. PPZ treatment increased the ratio of KIN10 to Histone3 in the nucleus of SLGCs. However, treatment with BL or Bikinin reduced the KIN10/ Histone3 ratio in the nucleus of SLGC (Figure S9). This regulation of the KIN10/ Histone3 ratio in the nucleus by BR signaling is consistent with the observed nuclear/cytoplasmic distribution of KIN10 in the SLGC (Figure S9). However, in the *kinβ2* mutant, the nuclear/cytoplasmic ratio of KIN10 were similar in M cells and SLGCs, also with PPZ and co-treatment with BL or Bikinin (Figure 4D and 4H). These data suggested that BR inhibited KIN10 nuclear localization in the leaf epidermal cells through the KINβ2 subunit.

To investigate how BR signaling modulates KIN10 subcellular localization and alters the stomatal lineage cell fate, we analyzed the subcellular localization of KIN10 and the cell identity marked by SPCH-RFP under PPZ treatment with or without BL or

Bikinin co-treatment. PPZ treatment enhanced both nuclear localized KIN10 intensity and SPCH-RFP intensity in SLGC cells. In contrast, BL or Bikinin treatment attenuated the PPZ-induced increases in both nuclear localized KIN10 intensity and SPCH-RFP cell fate identity in SLGC cells (Figure S10). These findings suggest that BR signaling also alter epidermal cell fate by inhibiting KIN10 nuclear localization. To determine whether the BIN2-KINβ2-KIN10 regulatory axis functions broadly in plant development, we detect endogenous KIN10 protein levels in purified nuclear and cytoplasmic fractions from whole-plant lysates of wild type and *kinβ2* mutant with or without BL treatment. In wild-type plants, BL treatment led to a reduction in nuclear KIN10 protein, indicating that BR signaling promotes the cytoplasmic retention of KIN10. Importantly, this BL-dependent decrease in nuclear KIN10 was reduced in *kinβ2* mutants, confirming that KINβ2 is crucial for BR-mediated regulation of KIN10 subcellular localization (Figure S11). These results indicated that the BIN2-KINβ2-KIN10 pathway is functional systemically, extending beyond stomatal lineages to influence broader aspects of plant growth and development.

BIN2 interacts with and phosphorylates KINβ2

Given that BIN2 activation by inhibition of BR signaling or by gain-of-function mutation can promote KIN10 nuclear localization through KINβ2, we speculated that BIN2 can directly interact with KINβ2. A strong YFP fluorescence signal in the cytosol of Arabidopsis mesophyll cell was observed in ratiometric bimolecular fluorescence complementation (rBiFC), when KINβ2-nYFP was co-transfected with BIN2-cYFP but not with histone H3-cYFP (Figure 5A). In protein pull-down assays, the glutathione S-transferase (GST) fusion protein GST-BIN2 interacted with the maltose-binding protein (MBP) fusion protein MBP-KINβ2 but not with MBP alone (Figure 5B). Co-immunoprecipitation (CoIP) assays using transgenic plants expressing BIN2-YFP under the native *BIN2* promoter and KINβ2-Myc under the 35S promoter confirmed the interaction between BIN2 and KINβ2 in plants (Figure 5C).

To determine whether KINβ2 regulates BIN2`s spatial polarity, we conducted the co-transformation assay of BASL-YFP and KINβ2-YFP in combination with BIN2-

RFP. The results revealed that BASL enhances the polarity of BIN2, while KINβ2 does not influence its polarized localization (Figure S12A and S12B). Additionally, the rBiFC assay revealed that the interaction of BIN2 and KINβ2 is localized to the plasma membrane, which is different with the polarized interaction between BIN2 and BASL (Figure S12C and S12D). This suggests that KINβ2 does not interfere with BIN2's polarized distribution.

Next, we investigated whether BIN2 could control KINβ2 function on stomatal development by phosphorylation. The *in vitro* kinase assays showed that MBP-BIN2 could phosphorylate MBP-KINβ2 directly but not MBP alone (Figure 5D). Mass spectrometry analysis revealed that BIN2 can phosphorylate the Serine-32, Serine-35, Serine-49 and Serine-53, which localized in the N-terminal variable region (NVR) of KINβ2, and the Serine-264 and Serine-270 residues in the C terminal domain (CTD) of KINβ2 (Figure S13A). Alignment analysis revealed that Serine-49 and Serine-53 are well conserved among plant species, whereas Serine-264 and Serine-270 only show limited conservation among dicotyledonous species (Figure S13B). We replaced all phosphorylated residues by alanine to generate the phospho-mutant KINβ2^{6A} protein. This protein displayed reduced P^{32} labelling signal in the *in vitro* kinase assay (Figure 5D), indicating that at least of these 6 phosphosites identified by mass spectrometry analysis are involved in BIN2-mediated phosphorylation of KINβ2. To investigate the function of BIN2-mediated KINβ2 phosphorylation in stomatal development, wild-type *KINβ2-YFP* and *KINβ2^{6A}-YFP were* transformed into *kinβ2* mutant (Figure S13C and S13D). KINβ2-YFP successfully restored the high stomatal index phenotype of *kinβ2* mutant. However, KINβ2^{6A}-YFP further reduced the stomatal index, also generating more epidermal cells (Figure 5E-5G). We also replaced phosphorylated residues by glutamate residues (KINβ2^{6D}) to mimic phosphorylation and generated 35 promoter driven KINβ2^{6D}-YFP transgenic plants (Figure S14A and S14B). While overexpression of wild type KINβ2 reduced the stomatal density and index in the wild-type background, *p35S::KINβ2^{6D}-YFP* failed to complement *kinβ2* mutant phenotype (Figure S14C and S14D). All these data suggested that BIN2 mediated phosphorylation regulates KINβ2

function on stomatal development negatively.

BIN2 dependent phosphorylation reduces KINβ2 membrane association and KINβ2 interaction with KIN10

Considering that KINβ2 displayed the increased dissociation from the plasma membrane in both M cells and SLGCs of in the *bin2-1* mutant, we speculated that BIN2 dependent phosphorylation maybe involved in the regulation of KINβ2 subcellular localization. We analyzed the intracellular protein levels of KINβ2-YFP or KINβ2^{6A}-YFP in M cells and SLGCs using the *pKINβ2::KINβ2-YFP* and *pKINβ2::KINβ2^{6A}-YFP* transgenic lines. The relative intracellular fluorescence intensity of KINβ2^{6A} was significantly lower than that of KINβ2 in both M cells and SLGCs. Specifically, the mean intensity of KINβ2^{6A} was 38.6% lower in M cells and 20.8% lower in SLGCs (Figure 5H and 5I). These findings suggested that BIN2-dependent phosphorylation is critical for KINβ2 membrane dissociation in M cells.

Given that BIN2 regulates the subcellular localization of KIN10 through the KINβ2-dependent manner, we next investigated whether BIN2-dependent phosphorylation of KINβ2 influences the interaction between KINβ2 and KIN10. We performed the *in vitro* protein pull down assays using GST-KIN10 to capture MBP-KINβ2 and phosphorylated MBP-KINβ2-P, phosphorylated by GST-BIN2 *in vitro* (Figure S15). The results showed that GST-KIN10 interacts with MBP-KINβ2 but not MBP alone. And interaction between GST-KIN10 and phosphorylated MBP-KINβ2-P was reduced compared with unphosphorylated MBP-KINβ2 (Figure 6A). To investigate the effects of phosphor-mutant and phosphor-mimic KINβ2 on its interaction with KIN10, we performed both *in vitro* protein pull-down assay and *in vivo* rBiFC assay. The *in vitro* protein pull-down assay showed that MBP-KINβ2^{6D} exhibited a weaker interaction with GST-KIN10, while MBP-KINβ2^{6A} showed a stronger binding (Figure 6B and 6C). The rBiFC assay further confirmed that KINβ2^{6D} inhibited interaction with KIN10, while KINβ2^{6A} enhances the binding with KIN10 (Figure S16A and S16B). Additionally, we performed a CoIP assay with with *pKINβ2::KINβ2-YFP* plants grown in PPZ containing medium with or without application of BL or

Bikinin. The results showed that both BL and Bikinin treatment enhance the interaction between KIN10 and KINβ2 (Figure 6D-6G). Together these data indicate that BIN2 dependent phosphorylation on KINβ2 also represses its interaction with KIN10.

Discussion

KIN10 has been shown to preferentially localize in nucleus of M cells and phosphorylate SPCH transcription factor to promote stomatal development. However, the regulatory mechanism of controlling KIN10's nuclear localization in M cells remains unclear. Here, we showed that BR reduces the nuclear localization of KIN10 by modulating KINβ2 through BIN2-mediated phosphorylation. In M cells, BIN2 is predominant and active in cytosol of M cells, phosphorylate KINβ2, which results in membrane dissociation of KINβ2 and reduction its interaction with KIN10, promoting the nuclear localization of KIN10. In SLGC and pavement cells, BIN2 turns to be inactive, leading to unphosphorylated KINβ2 membrane association and restrict KIN10 nuclear localization. Our results provide a new mechanism about how BIN2 modulating subcellular localization of KIN10 through KINβ2 to control M cells differentiation and stomatal development (Figure 7).

The SnRK1 complex serves as a metabolic sensor and regulator, enable plants to face diverse stress conditions as well as control their development in function of resource availability. Consistently, SnRK1 was found to be crucial role in controlling shoot and root apical meristem activity (Ramon et al., 2019; Lopes et al., 2024). In the root apical meristem, ABA triggers cytosolic SnRK1 inhibition of TOR kinase activity to limit root growth in stress conditions (Belda-Palazón et al., 2022). In the shoot apical meristem (SAM), knock down of *KIN10* expression by artificial microRNAs resulted in repression of *SHOOT MERISTEMLESS* (*STM*) expression and SAM development. Under energy-limiting low light or darkness conditions, KIN10 directly interacts with STM and repress STM controlled gene expression (Lopes et al., 2024). In addition, the KIN10-bZIP63 module, known to regulate metabolic gene expression under energy stress conditions, is also expressed in lateral root primordia and responsible for *AUXIN*

RESPONSE FACTOR19 (*ARF19*) induction under energy deficiency to prime lateral root initiation (Muralidhara et al., 2021). Our study now further demonstrates that SnRK1 is also essential for meristemoid differentiation into stomata in Arabidopsis. The Arabidopsis leaf epidermis possesses tremendous plasticity owing to the stem cell-like characteristics of MMC and M cells. M cells undergo continuous asymmetric divisions to generating more stomatal lineage cells or differentiate into GMC cells to generate stomata (Bergmann and Sack, 2007). This fate determination of M cells controls the amount of leaf epidermal cells and stomata with sufficient space for optimal functioning. The SPCH to MUTE transition (with SPCH inducing MUTE expression) is a key event for M cell fate determination (Lau et al.,2014; Han et al.,2018; Lopez-Anido et al., 2021). However, the factors determining the timing of this transition are still unknown. Interestingly, while KIN10 predominantly localizes in the nucleus in M cells, KINβ2 exhibits membrane dissociation and cytosolic localization. Interfering with KIN10 nuclear localization or enhancing KINβ2 membrane association by genetic manipulation leads to epidermal cell proliferation or deficient stomata formation. *kin10*$^{+/-}$ *kin11*$^{+/-}$ mutant and *myrKIN10 kin10 kin11* complemented plants exhibit more epidermal cells and a higher proportion of anisocytic stomatal complexes with more than four cells, indicating that nuclear localization of KIN10 results in less rounds of M cell division and benefits M cell differentiation. Previous study showed that KIN10 catalyzes the phosphorylation of N termination of SPCH in the nucleus of M cells (Han et al., 2020). Mutation KIN10 dependent phosphosites leads to extreme less amounts of stomata, which is quite different with other SPCH phosphosite mutation (Han et al., 2020). Both BIN2 and MPK3/6 kinase could phosphorylate SPCH and tun it unstable. However, the mutation of BIN2 and MPK3/6 dependent phosphosites on SPCH results in much more amounts of epidermal cells (Gudesblat et al., 2012; Lampard et al., 2008). It seems that BIN2 and MPK3/6 dependent phosphorylation regulates SPCH mediated cell proliferation, whereas KIN10 dependent phosphorylation regulates SPCH mediated cell fate transition. Notably, recent advance showed that the cell size of M cells is the key threshold for differentiation. During M cell shrinkage of consistent

divisions, the key regulatory factors from nucleus is concentrated and trigger the M cell fate transition (Gong et al., 2023). It is worthy to check whether KIN10 nuclear localization and KIN10 dependent phosphorylation on SPCH is regulated by M cells size shrinkage.

The SnRK1 catalytic subunits are nucleo-cytosolic proteins and dynamic subcellular localization is an important mechanism for plant SnRK1 activity regulation. SnRK1 is an atypical AMPK family kinase. Rather than being activated by low nucleotide charge (increased AMP and ADP to ATP ratio), SnRK1 appears to be active by default and repressed by sugar-phosphates (Han et al., 2024; Ramon et al., 2019). Because of its default activity, nuclear translocation of KIN10 is sufficient to induce target gene expression under energy stress conditions (Ramon et al., 2019; Pierre et al., 2007). The N-terminally myristoylated and membrane-associated KINβ subunits play a critical regulatory role in limiting KIN10 nuclear translocation, which has dramatic effects on metabolic stress response as well as plant development (Ramon et al., 2019; Pierre et al., 2007). Recently, additional factors were reported to regulate KIN10 localization. Notably, ABA treatment leads to KIN10 nuclear export in the root meristem to inhibit cytosolic TOR kinase activity and thus root growth (Belda-Palazón et al., 2022). Interactomics analyses also revealed and extended SnRK1 complex with several tightly interacting plant-specific regulatory proteins, including the class II trehalose-6-phosphate synthase (TPS)-like proteins, which also inhibit KIN10 nuclear localization through its sequestration at the endoplasmic reticulum (Van Leene et al., 2022). We previous showed that H_2O_2, a key signaling of reactive oxygen species, interferes with the interaction between KINβ2 and KIN10, which facilitates the nuclear localization of KIN10 in M cells and guard cells (Shi et al., 2024; Shi et al., 2022). Here, we showed that BIN2, the negative regulator in BR signaling, phosphorylates KINβ2 and releases its interaction with KIN10, promoting KIN10 nuclear localization in stomatal lineage cells.

BR is an important steroid phytohormone involved in regulating plant development. Recent studies revealed that BR biosynthesis genes exhibit specific

expression patterns in different layers or developmental zones of root tip tissues, which maximize BR concentration in the elongation zone to benefit root growth (Vukašinović et al., 2021; Vukašinović et al., 2025). BR metabolic precursors also relies on the cell-to-cell movement through plasmodesmata between root cells (Wang et al., 2023). Similar to its role in root tissues, BR signaling also exhibits cell-specificity in the epidermis, notably controlling stomatal development in different tissues (Kim et al., 2012; Gudesblat et al., 2012; Wang et al., 2015; Park et al., 2025). BIN2, as negative regulator of BR signaling, remains cytosolic in M cells but localizes to the nucleus in SLGCs (Houbaert et al., 2018; Guo et al., 2021). In M cells, BIN2 phosphorylates and represses the MAPKKK kinase YODA, as well as the phosphorylation of MPK3 and MPK6, which negatively regulates stomatal development and promotes SPCH stability and M cell division (Kim et al., 2012). POLAR and its closest homolog POLAR-LIKE1 interact with BIN2 and protect it from BL-mediated inactivation, keeping BIN2 active in M and asymmetric cell division precursors (Kim et al., 2023). In SLGCs, the polarized protein phosphatase BSL1 promotes BIN2`s partitioning into the nucleus, where BIN2 phosphorylates SPCH and destabilizes it (Guo et al., 2021; Gudesblat et al., 2012). Here, we show that BR signaling limits KIN10 nuclear localization through its interaction with KINβ2 and membrane association. Specifically, BIN2 interacts with and phosphorylates KINβ2, which reduces KINβ2 membrane association and its interaction with KIN10. BIN2 activation in M cells facilitates KIN10 nuclear localization, subsequent phosphorylation and stabilization of SPCH, which promotes M cells differentiating into stomata. Consistent with this, Bikinin is more effective in promoting KINβ2 membrane association in M cells compared to BL treatment. However, both Bikinin and BL treatment fail to repress KIN10 nuclear localization in M cells. One possible explanation for this is that hydrogen peroxide (H_2O_2) always accumulates in M cells, interfering with the interaction between KINβ2 and KIN10 (Shi et al., 2022). This suggest that H_2O_2 and BIN2-mediated phosphorylation are two independent pathways to regulate SnRK1 complex assembly and subcellular localization.

These findings indicate that SnRK1 is generally involved in the control of plant stem cell activity and differentiation. Our findings indicate that shifting subcellular localization of SnRK1 is a key regulatory mechanism in epidermal stem cell fate determination, which is intricately regulated by diverse metabolic and phytohormone signals.

Material and Methods

Plant material and growing conditions

The Arabidopsis wild-type seedling and all mutants and transgenic plants used in this study have a Columbia (Col-0) ecotype background. The mutants and transgenic plants used in this study include *kin10* (GABI_579_E09)(Ramon et al., 2019; Han et al., 2020), *kin11* (WiscDsLox320B03))(Ramon et al., 2019; Han et al., 2020), *KIN10-flag kin10kin11*(Ramon et al., 2019), *nlsKIN10-flag kin10kin11*(Ramon et al., 2019), *myrKIN10-flag kin10kin1*(Ramon et al., 2019), *pKIN10::KIN10-YFP*(Han et al., 2020), *kinβ2-1* (SALK_037416C)(Shi et al., 2024), *kinβ2-2* (SALK_052521) (Shi et al., 2024), *p35S::KINβ2-YFP*(Shi et al., 2024), *det2-1* (Li et al., 1996), *bin2-1*(Peng et al., 2008) and *bri1-116* (Wang et al., 2002)have been described previously. *kinβ1-2* (SALK_135746) and *kinβ3* (SALK-202587C) were ordered from the Arabidopsis Biological Resource Center. The transgenic construct of *pKINβ2::KINβ2-YFP*, *pKINβ2::KINβ2^{6A}-YFP, pSPCH::KINβ2-YFP*, *pSPCH::myr-KINβ2-YFP and p35S::KINβ2^{6D}-YFP* were transferred into the *kinβ2* (SALK_037416C) background for phenotypic analysis.

Seeds of Arabidopsis were sterilized with 70% ethanol containing 0.1% Triton X-100 and washed in 100% ethanol. Sterilized seeds were cold stratified at 4℃ for 2 days. Depending on the purpose of experiments, 10 nM brassinolide (BL), 30 μM Bikinin, or 2 μM propiconazole (PPZ) were added to 1/2 Murashige and Skoog (MS) medium. To analyze the stomatal developmental phenotypes, seedlings of wild-type, mutants and transgenic plants were grown on 1/2 MS medium under 12-hour light/12-hour dark photoperiod with 80μmol m^{-2} s^{-1} light intensity at 22 °C for 9 days.

Plasmid construction.

The coding regions of *KINβ2* and *BIN2* were amplified and inserted into pENTR/SD/D-TOPO vectors (Thermo Fisher) and transferred into destination vectors Px-YFP (p35S:X-YFP), p1390-MH (p35S:X-Myc-His), pGAL4ADGW (GAL4AD-X), pGAL4BDGW (GAL4BD-X), pMAL2CGW (MBP-X) and pDEST15 (X-GST). The constructs of BIN2 dependent phosphosites mutation of $KINβ2^{6A}$ and $KINβ2^{6D}$ were created using the fast mutagenesis system kit (TransGen). Oligo primers used for cloning are listed in Supplementary Table 1. The binary vector constructs were introduced into Agrobacterium tumefaciens (strain GV3101), and the floral dipping method was used to transform them into Col-0 wild type or *kinβ2* (SALK_037416C) plants.

Stomatal quantification

For stomatal quantification, the abaxial epidermis of Arabidopsis cotyledons for stomatal quantification was cleared by decolor solution (75% ethanol 25% acetic acid) for 6 h or overnight. Cotyledons were captured and dried on paper, then submerge into Hoyer's solution (5% Arabic Gum; 70% Chloral hydrate; 4% Glycerol) until cotyledons turned completely transparent for microscopic observation. 700 μm × 550μm images from central regions of abaxial cotyledons were captured by using a microscope (Olympus BX53). Guard cells, dividing small cells and pavement cells were counted for stomatal index calculation. The pictures of abaxial cotyledon epidermises were edited in Adobe Illustrator software based on DIC picture. The size of epidermal cells was calculated by ImageJ software. Statistical analysis results were showed in Supplementary Table 2.

Confocal Microscopy

Confocal microscopy was performed using an LSM-880 laser scanning confocal microscope (Zeiss) or STELLARIS5 confocal microscope (Leica) for detecting KIN10 and KINβ2 protein subcellular localization. Transgenic plants with KIN10-YFP or KINβ2-YFP was were grown on 1/2 MS medium under 12-hour light/12-hour dark photoperiod with 80 μmol m^{-2} s^{-1} light intensity at 22 °C for 3 days. The abaxial

epidermis of 3 days old Arabidopsis cotyledons was stained with Propidium Iodide (PI) staining to visualize cell outline. Images were captured at 488 nm and 515 nm laser excitation for YFP and PI, respectively. Emission filters were set as 490 to 560 nm for YFP and as 580 to 660 nm for PI. Two channels were excited sequentially. RFP fusion protein images were captured at 515nm laser excitation and 580 to 660nm for emission. The average gray values of nuclear and cytoplasmic KIN10-YFP were quantified by Image J software and used for calculating KIN10 nuclear/cytoplasmic ratio. The average gray value of intracellular KINβ2-YFP were quantified by Image J software and normalized by average gray value of pavement cells in every image, which was used for calculating intracellular fluorescence intensity of KINβ2-YFP. Statistical analysis results were showed in Supplementary Table 2.

Ratiometric bimolecular fluorescence complementation assay

The coding sequences of *KINβ2* and *BIN2* were amplified from full length complementary DNA (cDNA) by PCR and cloned using BP recombination reaction (Invitrogen, Carlsbad, CA, USA) into the pDONR221-P_1P_4 or pDONR221-P_2P_3 vectors, respectively. After LR reactions, the coding sequences of *KINβ2* and *BIN2* were recombined into destination vector pBiFC-2in1-NN to generate the expression construct with *p35S:nYFP-KINβ2-p35S:RFP-p35S:cYFP-BIN2*. *p35S:nYFP-KINβ2-p35S:RFP-p35S:cYFP-Histone3* was constructed and used as control. Agrobacterial suspensions with this construct were injected into tobacco leaves. The transfected plants were kept in a greenhouse for 36 h at 22°C.Fluorescent signals were visualized using a LSM-880 laser scanning confocal microscope (Zeiss). Images were captured at 488 nm and 515nm laser excitation for YFP and RFP, respectively. Emission filters were set as 490 to 560 nm for YFP and as 580 to 660 nm for RFP. Two channels were excited sequentially.

***In vitro* pull-down assay.**

For the *in vitro* pull-down assay, KINβ2 fused with an MBP tag and BIN2 fused with GST tag were purified from bacteria using amylose resin (NEB) and glutathione beads (GE Healthcare), respectively. GST-BIN2 (1 μg) was incubated with MBP-

KINβ2 (1 μg) or MBP (1 μg) in pull-down buffer (20 mM HEPES pH 7.5, 40 mM KCl, 5 mM EDTA, 0.05% Triton X-100) for 1 h at room temperature. Then, the beads were washed nine times using the wash buffer (20 mM HEPES pH 7.5, 40 mM KCl, 5 mM EDTA, 300 mM NaCl, 0.1% Triton X-100). Total proteins were eluted from the beads by boiling in 2× sodium dodecyl sulfate (SDS), loaded and separated on an 8% SDS-polyacrylamide gel. The gel blots were analyzed using anti-GST (TransGen Biotech, Cat: HT601-01,1:5000 dilution) and anti-MBP (TransGen Biotech, Cat: HT701-01,1:5000 dilution).

***In vivo* Co-IP assay.**

pBIN2:BIN2-GFP p35S::KINβ2-Myc and *p35S::KINβ2-Myc* seedlings were grown on the 1/2 MS medium under 12-hour light/12-hour dark photoperiod with 80μMol $m^{-2\ -1}$ light intensity at 22 °C for 10 days. *p35S:: KINβ2-Myc* seedling were used as control. Total proteins were extracted from the tissues using immunoprecipitation buffer (40 mM KCl, 20 mM HEPES pH 7.5, 5 mM EDTA, 0.05% Triton X-100 and 1× protease inhibitor from Sigma Aldrich, 1 mM Phenylmethanesulfonyl fluoride). Co-immunoprecipitation was performed using homemade GFP-trap beads and immunoblotted using anti-GFP (TransGen, Cat: N20610, 1:5,000 dilution) and mouse anti-Myc (Sigma Aldrich, 1:5,000 dilution).

***In vitro* kinase assay, mass spectrometry and phosphopeptide analysis.**

MBP-KINβ2, GST-BIN2 and MBP-KINβ2^{6A} proteins were purified from Escherichia coli strain BL21. GST-BIN2 proteins were incubated with MBP-KINβ2 or MBP- KINβ2^{6A} proteins in kinase buffer (20 mM Tris-HCl pH 7.5, 1 mM $MgCl_2$, 100 mM NaCl, 1 mM Dithiothreitol and 10 μM cold ATP) containing (γ-32P) ATP (1 μCi) at 30 °C for 1 h. SDS buffer (5×) was added to stop the reaction. Proteins were separated by 8% SDS-PAGE and then digested with trypsin after non-radioactive *in vitro* kinase assays. The digested peptide mixtures were desalted and separated using a Thermo U3000 nano RSLC system (Thermo Fisher) before analysis using a Q Exactive HF Hybrid Quadrupole-Orbitrap mass spectrometer (Thermo Fisher). The phosphorylated residues in MBP-KINβ2 were identified by PEAKS Studio Xplus software.

628

629 **Data and code availability**

630 All data are provided in the main or supplementary text. Any additional information
631 required to reanalyze the data reported in this paper is available from the lead contact
632 upon request. This paper does not report original code.

633

634 **Figure Legend**

635 **Figure 1. Nuclear localized KIN10 is required for Meristemoid differentiation.**
636 (A and B). The Subcellular localization of KIN10 protein in abaxial epidermis of
637 Arabidopsis cotyledons. The *pKIN10::KIN10-YFP p35S::Histone3-RFP* transgenic
638 line was grown on 1/2 MS medium under 12-hour light/12-hour dark photoperiod with
639 80 μmol m^{-2} s^{-1} light intensity for 3 days. Confocal images (A) and line scan analysis
640 (B) of KIN10-YFP in abaxial epidermis were performed. Histone3-RFP was set as
641 reference protein in nucleus. Nuc indicates nucleus, Mem indicates plasma membrane.
642 The fluorescent signals of KIN10-YFP protein are in green. Histone3-RFP are in purple.
643 Scale bars in confocal images represent 20μm.
644 (C-E). Quantification of the stomatal index (D) and density of total epidermal cells (E)
645 of wild-type plants, *kin10* mutant, *kin10-/- kin11+/-* loss-of-function sesqui-mutant,
646 *KIN10-flag kin10 kin11*, *nlsKIN10-flag kin10 kin11* and *myrKIN10-flag kin10 kin11*
647 transgenic lines. Plants material were grown on 1/2 MS medium under 12-hour light/12-
648 hour dark photoperiod with 80 μmol m^{-2} s^{-1} light intensity for 9 days. Cell size
649 distribution of representative images of abaxial epidermis is presented as a color scale
650 (C). Error bars indicate standard deviation (S.D.) (n=20). Different letters above the
651 bars indicate statistically significant differences between samples (One-way ANOVA
652 analysis followed by Uncorrected Fisher's LSD multiple comparisons test, $p < 0.05$).
653 **Figure 2. Plasma membrane-dissociated localization of KINβ2 in epidermis is**
654 **correlated with KIN10 nuclear localization and crucial for stomatal development.**
655 (A and B). The Subcellular localization of KINβ2 and KIN10 protein in abaxial
656 epidermis of Arabidopsis cotyledons. The *pKINβ2::KINβ2-YFP p35S::Histone3-RFP*

and *pKIN10::KIN10-YFP p35S::Histone3-RFP* transgenic lines were grown on 1/2 MS medium under 12-hour light/12-hour dark photoperiod with 80 μmol m^{-2} s^{-1} light intensity for 3 days. Confocal images of KINβ2-YFP and KIN10-YFP in different types of epidermal cells were shown (A). Histone3-RFP was set as reference protein in nucleus. The fluorescent signals of KIN10-YFP and KINβ2-YFP protein are in green. Histone3-RFP is in purple. The intracellular fraction of protein intensity of KINβ2-YFP and ratio of nuclear and cytoplasmic ratio of KIN10-YFP in different types of epidermal cells were quantified (B). The solid lines of violin plots represent median, the dashed lines represent first or third quartile. Scale bars in confocal images represent 20 μm.

(C-D). KINβ2 regulates KIN10 nuclear localization in stomatal developmental cells. The *pKIN10::KIN10-YFP* and *pKIN10::KIN10-YFP kinβ2* transgenic lines were grown on 1/2 MS medium under 12-hour light/12-hour dark photoperiod with 80 μmol m^{-2} s^{-1} light intensity for 3 days. The nuclear/cytoplasmic ratio of KIN10-YFP in M cells and SLGCs after asymmetric divisions were calculated (D). The fluorescent signals of KIN10-YFP protein are in green, PI-marked cell outlines are in purple. Scale bars in confocal images represent 20 μm. Number above bars indicate ratio of medium value between bars. The solid lines of violin plots represent median, the dashed lines represent first or third quartile (n=200). Different letters above the bars indicate statistically significant differences between samples (Two-way ANOVA analysis followed by Tukey's multiple comparisons test, $p < 0.05$). Scale bars in confocal images represent 20 μm.

(E-G). Quantification of the stomatal index (F) and stomatal density (G) of wild-type plants, *kinβ2* mutant, *pSPCH::KINβ2-RFP kinβ2* and *pSPCH::myrKINβ2-RFP kinβ2* transgenic lines. Plants material were grown on 1/2 MS medium under 12-hour light/12-hour dark photoperiod with 80 μmol m^{-2} s^{-1} light intensity for 3 or 9 days. The fluorescent signals of KINβ2-RFP with different localization isoform in abaxial epidermis of 3 days old seedlings were in green (E). Error bars indicate standard deviation (S.D.) (n=20). Different letters above the bars indicate statistically significant differences between samples (One-way ANOVA analysis followed by Uncorrected

Fisher's LSD multiple comparisons test, $p < 0.05$). Scale bars in confocal images represent 20 μm.

Figure 3. SnRK1 complex is involved in BR regulated stomatal development.

(A-C). Quantification of the stomatal index (B) and stomatal density (C) of wild-type plants, *kin10* mutant, *bin2-1* mutant, *bri1-116* mutant, *bin2-1 kin10* double mutant and *bri1-116 kin10* double mutant. Plants material were grown on 1/2 MS medium under 12-hour light/12-hour dark photoperiod with 80 μmol m^{-2} s^{-1} light intensity for 9 days.

(D and E). Quantification of the stomatal index (D) and stomatal density (E) of wild-type plants, *KINβ2-Ox* (*p35S::KINβ2-YFP 5#*), *bri1-116* mutant and *bri1-116 KINβ2-Ox* cross line. Plants material were grown on 1/2 MS medium under 12-hour light/12-hour dark photoperiod with 80 μmol m^{-2} s^{-1} light intensity for 9 days.

Cell size distribution of representative images of abaxial epidermis is presented as a color scale (A). Error bars indicate standard deviation (S.D.) (n=20). Different letters above the bars indicate statistically significant differences between samples (One-way ANOVA analysis followed by Uncorrected Fisher's LSD multiple comparisons test, $p < 0.05$).

Figure 4. BR signaling promotes the plasma membrane association of KINβ2 and represses KIN10 nuclear localization through KINβ2.

(A and B). Plasma membrane disassociated of KINβ2-YFP in SLGCs of *bri1-116* and *bin2-1* mutant was enhanced. The *pKINβ2::KINβ2-YFP, pKINβ2::KINβ2-YFP bri1-116, pKINβ2::KINβ2-YFP bin2-1* transgenic line was grown on 1/2 MS medium under 12-hour light/12-hour dark photoperiod with 80 μmol m^{-2} s^{-1} light intensity for 3 days. The confocal images of different lines were shown (A). The relative intracellular KINβ2-YFP intensity of M cells and SLGCs after asymmetric divisions under different genetic background were calculated (B).

(C and D). BL and Bikinin prevent PPZ-induced plasma membrane disassociation of KINβ2-YFP in SLGCs. The *pKINβ2::KINβ2-YFP* transgenic line was grown on 1/2 MS medium with or without 2μM PPZ under 12-hour light/12-hour dark photoperiod with 80μmol m^{-2} s^{-1} light intensity for 2 days. And seedling grown on PPZ medium were

transferred to 1/2 MS medium containing Mock solution, 10 nM BL or 30 μM Bikinin (BIK) for 24 hours. The confocal images under different conditions was shown (C). The relative intracellular KINβ2-YFP intensity of M cells and SLGCs after asymmetric divisions under different condition were calculated (D).

The fluorescent signals of KINβ2-YFP protein are in green, PI-marked cell outlines are in purple. Scale bars in confocal images represent 20μm. The solid lines of violin plots represent median, the dashed lines represent first or third quartile. Different letters above the bars indicate statistically significant differences between samples (Two-way ANOVA analysis followed by Tukey's multiple comparisons test, $p < 0.05$).

(E and F). BR signaling mutants *bri1-116* and *bin2-1*, BR biosynthesis mutant *det2-1* promote nuclear localization of KIN10-YFP in SLGCs. The *pKIN10::KIN10-YFP, pKIN10::KIN10-YFP bri1-116, pKIN10::KIN10-YFP bin2-1* and *pKIN10::KIN10-YFP det2-1* transgenic lines were grown on 1/2 MS medium under 12-hour light/12-hour dark photoperiod with 80 μmol m^{-2} s^{-1} light intensity for 3 days. The confocal images of wild type and mutants background of KIN10-YFP was shown (E). The nuclear/cytoplasmic ratio of KIN10-YFP in M cells and SLGCs after asymmetric divisions under different genetic background were calculated (F).

(G and H). BL and Bikinin prevent PPZ-induced nuclear localization of KIN10-YFP in SLGCs through KINβ2. The *pKIN10::KIN10-YFP* and *pKIN10::KIN10-YFP kinβ2* transgenic lines were grown on 1/2 MS medium with or without 2 μM PPZ under 12-hour light/12-hour dark photoperiod with 80 μmol m^{-2} s^{-1} light intensity for 3 days. And seedling grown on PPZ medium were transferred to 1/2 MS medium containing Mock solution, 10 nM BL or 30 μM Bikinin (BIK) for 3 hours. The confocal images of wild type background and *kinβ2* mutant under different treatment conditions was shown (G). The nuclear/cytoplasmic ratio of KIN10-YFP in M cells and SLGCs after asymmetric divisions under different treatment conditions were calculated (H).

The fluorescent signals of KIN10-YFP protein are in green, PI-marked cell outlines are in purple. Scale bars in confocal images represent 20 μm. The solid lines of violin plots represent median, the dashed lines represent first or third quartile (n=200). Different

letters above the bars indicate statistically significant differences between samples (Two-way ANOVA analysis followed by Tukey's multiple comparisons test, $p < 0.05$).

Figure 5. BIN2 interacts with and phosphorylates KINβ2 to promote KINβ2 membrane dissociation

(A-C). Ratiometric BiFC (A), *in vitro* pull-down (B), and CoIP (C) assays show the interaction between BIN2 and KINβ2. The *p35S:nYFP-KINβ2-p35S:RFP-p35S:cYFP-Histone3* construct was set as negative control. Scale bars in confocal images of ratiometric BiFC represent 10 μm. In pull-down assay, recombinant MBP and MBP-KINβ2 proteins were incubated with GST-BIN2 bound to glutathione agarose beads. Immunoblot assay was performed with anti-MBP antibody to detect the proteins bound to GST-BIN2. Protein extract from 10-day-old seedlings of *p35S::KINβ2-Myc pBIN2::BIN2-YFP* and *p35S::KINβ2-Myc* plants were used for CoIP assay. BIN2-YFP was precipitated using GFP-Trap agarose beads. The immunoblots were probed with anti-GFP and anti-Myc antibodies.

(D). BIN2 phosphorylates KINβ2 *in vitro*. Upper panel showed gel image with ATP-γ-p32-labeled proteins. Bottom panel showed gel image stained with Coomassie brilliant blue.

(E-G). Quantification of the stomatal index (E) and total epidermal cell density (F) of wild-type plants, *kinβ2* mutant and different KINβ2-complemented transgenic plants. Cell size distribution of representative images of abaxial epidermis is presented as a color scale (G). Plants were grown on 1/2 MS medium under 12-hour light/12-hour dark photoperiod with 80 μmol m^{-2} s^{-1} light intensity for 9 days. Error bars indicate standard deviation (S.D.) (n=20). Different letters above the bars indicate statistically significant differences between samples (One-way ANOVA analysis followed by Uncorrected Fisher's LSD multiple comparisons test, $p < 0.05$).

(H and I). The BIN2-dependent phosphosites mutation enhances the KINβ2 membrane association. The *pKINβ2::KINβ2-YFP kinβ2* and *pKINβ2::KINβ2^{6A}-YFP kinβ2* transgenic line were grown on 1/2 MS medium under 12-hour light/12-hour dark photoperiod with 80 μmol m^{-2} s^{-1} light intensity for 3 days. The confocal images of

KINβ2-YFP and KINβ2^{6A}-YFP was shown (H). The fluorescent intensity of intracellular KINβ2-YFP and KINβ2^{6A}-YFP in M cells and SLGCs were quantified (I). The solid lines of violin plots represent median, the dashed lines represent first or third quartile. Different letters above the bars indicate statistically significant differences between samples (Two-way ANOVA analysis followed by Tukey's multiple comparisons test, $p < 0.05$).

Figure 6. BIN2 dependent phosphorylation fine tunes KINβ2's interaction with KIN10.

(A-C). *In vitro* protein pull-down assay showed that phosphorylated KINβ2 by BIN2 weaken the interaction with KIN10 through BIN2 dependent phosphosites. GST-BIN2 bound to glutathione agarose beads was performed *in vitro* kinase assay with MBP-KINβ2 first. And phosphorylated and unphosphorylated MBP-KINβ2 were incubated with GST-KIN10 bound to glutathione agarose beads (A). Recombinant MBP, MBP-KINβ2, MBP-KINβ2^{6A} and MBP-KINβ2^{6D} proteins were incubated with GST-KIN10 bound to glutathione agarose beads. Immunoblot assay was performed with anti-MBP antibody to detect the proteins bound to GST-KIN10.

(D-G). *In vivo* CoIP assay showed that BL and Bikinin enhance the interaction of KINβ2 and KIN10. *pKINβ2::KINβ2-YFP* transgenic line were grown on 1/2 MS medium containing 2 μM PPZ under 12-hour light/12-hour dark photoperiod with 80μmol m^{-2} s^{-1} light intensity for 9 days. And seedling grown were transferred to 1/2 MS medium containing Mock solution, 10 nM BL (D, E) or 30 μM Bikinin (BIK) (F-G) for 0.5 or 2 hours. KINβ2-YFP was precipitated using GFP-Trap agarose beads. The interaction with KIN10 were detect by anti-KIN10 antibody. The relative fold change of immunoprecipitated MBP-KINβ2 or KIN10 compared with Input was calculated by ImageJ software. Error bars indicate standard deviation (S.D.) of three biological repeats. Different letters above the bars indicate statistically significant differences between samples (One-way ANOVA followed by Tukey's multiple comparisons test, $p < 0.05$).

Figure 7. A proposed working model for BIN2 regulates SnRK1 complex

subcellular localization and stomata development. In meristemoid cells, BIN2 keeps activating and phosphorylates KINβ2, which promotes membrane dissociation of KINβ2 and releasing the interaction with KIN10. KIN10 translocates into nucleus and phosphorylates SPCH to benefit meristemoid cells differentiating into stomata. In SLGCs, BIN2 turns to be less active. KINβ2 keeps interaction with KIN10 and membrane association, which induces the nuclear localization of KIN10, SPCH unstable and more cells surrounded stomata. In contrast, the deficient of BR biosynthesis or signaling transduction enhances BIN2 activity in SLGCs, leading to the nuclear localization of KIN10, SPCH stable and higher density of stomata.

Author Contributions

L.-M. Y., C.H. and M.-Y. B together designed the experiments. L.-M. Y. and C.H. performed stomatal developmental phenotype analysis and subcellular observation of SnRK1 complex subunit by confocal images. L.-M. Y. and C.H. performed kinase assays and mass spectrometer analysis. L.-M. Y. performed RT-PCR, western blot, protein pull down assay and rBiFC analysis and all other experiment. L.-M. Y. generated *KINβ2-Ox bri1-116*, *kin10 bin2-1*, *kin10 bri1-116* and different subcellular localized KINβ2 and KINβ2 site-mutant rescue lines. W. S., Y.-X. G, and L.-M. Y. together cross and generate *kinβ1-2 kinβ2-1*, *kinβ1-2 kinβ2-1*, *kinβ-t* (*kinβ1-2 kinβ2-2 kinβ3*) mutants. F. R. provides *KIN10-flag kin10 kin11*, *nlsKIN10-flag kin10 kin11* and *myrKIN10-flag kin10 kin11*transgenic lines and critical discussion for manuscript. F.M. and M.-Y. B provides suggestion for experimental design and writing. C.H. and M.-Y. B wrote the manuscript.

Acknowledgement

We thank Haiyan Yu, Yuyu Guo and Xiaomin Zhao from the Analysis and Testing Center of SKLMT (State Key Laboratory of Microbial Technology, Shandong University) for assistance with the LSM-880 laser scanning confocal microscope (Zeiss). We also thanks Yiteng Xu from the Core Facility and Service Platform at

School of Life Sciences, Shandong University for the assistance provided in laser scanning STELLARIS5 confocal microscope (Leica) imaging. This work was supported by grants from the National Natural Science Foundation of China (32270351 to C.H., 32325006 to M.-Y.B., U24A20389 to M.-Y.B., 32461160287 to M.-Y.B.), Agricultural Variety Improvement Project of Shandong Province (2022LZGC001 to M.-Y.B., 2024LZGC007 to M.F.) and Science and Technology Department of Shandong Province (ZR2022YQ20 to C.H.).

Reference:

Adam, S.A., Lobl, T.J., Mitchell, M.A., Gerace, L. (1989). Identification of specific binding proteins for a nuclear location sequence. Nature **337**: 276-279.

Belda-Palazón, B., Costa, M., Beeckman, T., Rolland, F., Baena-González, E. (2022). ABA represses TOR and root meristem activity through nuclear exit of the SnRK1 kinase. Proc. Natl. Acad. Sci. USA **119**: e2204862119.

Bergmann, D.C., and Sack, F.D. (2007). Stomatal development. Annu. Rev. Plant Biol. **58**: 163-181.

Broeckx, T., Hulsmans, S., and Rolland, F. (2016). The plant energy sensor: evolutionary conservation and divergence of SnRK1 structure, regulation, and function. J. Exp. Bot. **67**: 6215-6252.

Emanuelle, S., Hossain, M.I., Moller, I.E., Pedersen, H.L., van de Meene, A.M., Doblin, M.S., Koay, A., Oakhill, J.S., Scott, J.W., Willats, W.G., et al. (2015). SnRK1 from Arabidopsis thaliana is an atypical AMPK. Plant J. **82**: 183-192.

Gong, Y., Dale, R., Fung, H.F., Amador, G.O., Smit, M.E., Bergmann, D.C. (2023). A cell size threshold triggers commitment to stomatal fate in Arabidopsis. Sci. Adv. **9**: adf3497.

Gudesblat, G.E., Schneider-Pizoń, J., Betti, C., Mayerhofer, J., Vanhoutte, I., van Dongen, W., Boeren, S., Zhiponova, M., de Vries, S., Jonak, C., Russinova, E. (2012). SPEECHLESS integrates brassinosteroid and stomata signalling pathways. Nat.

Cell Biol. **14**: 548-554.

Guo, X., Park, C.H., Wang, Z.Y., Nickels, B.E., Dong, J. (2021). A spatiotemporal molecular switch governs plant asymmetric cell division. Nat. Plants **7**: 667-680.

Han, C., Liu, Y., Shi, W., Qiao, Y., Wang, L., Tian, Y., Fan, M., Deng, Z., Lau, O.S., De Jaeger, G., et al. (2020). KIN10 promotes stomatal development through stabilization of the SPEECHLESS transcription factor. Nat. Commun. **11**: 4214.

Han, C., Wang, H. L., Shi, W. Bai, M. Y. (2024). The molecular associations between the SnRK1 complex and carbon/nitrogen metabolism in plants. N. Crops **1**: 100008.

Han, C., Wang, L., Lyu, J., Shi, W., Yao, L., Fan, M., Bai, M.Y. (2023). Brassinosteroid signaling and molecular crosstalk with nutrients in plants. J. Genet. Genomics **50**: 541-553.

Han, S.K., Qi, X., Sugihara, K., Dang, J.H., Endo, T.A., Miller, K.L., Kim, E.D., Miura, T., Torii, K.U. (2018). MUTE directly orchestrates cell-state switch and the single symmetric division to create stomata. Dev Cell. **45**: 303-315.

Heidstra, R., and Sabatini, S. (2014). Plant and animal stem cells: similar yet different. Nat. Rev. Mol. Cell Biol. **15**: 301-312.

Houbaert, A., Zhang, C., Tiwari, M., Wang, K., de Marcos Serrano, A., Savatin, D.V., Urs, M.J., Zhiponova, M.K., Gudesblat, G.E., Vanhoutte, I., Eeckhout, D., et al. (2018). POLAR-guided signalling complex assembly and localization drive asymmetric cell division. Nature **563**: 574-578.

Kim, E.J., Zhang, C., Guo, B., Eekhout, T., Houbaert, A., Wendrich, J.R., Vandamme, N., Tiwari, M., Simon-Vezo, C., Vanhoutte, I., et al. (2023). Cell type-specific attenuation of brassinosteroid signaling precedes stomatal asymmetric cell division. Proc. Natl. Acad. Sci. USA **120**: e2303758120.

Kim, T.W., and Wang, Z.Y. (2010). Brassinosteroid signal transduction from receptor kinases to transcription factors. Annu. Rev. Plant Biol. **61**: 681-704.

Kim, T.W., Michniewicz, M., Bergmann, D.C., Wang, Z.Y. (2012). Brassinosteroid regulates stomatal development by GSK3-mediated inhibition of a MAPK pathway. Nature **482**: 419-422.

Lampard, G.R., Macalister, C.A., and Bergmann, D.C. (2008). Arabidopsis stomatal initiation is controlled by MAPK-mediated regulation of the bHLH SPEECHLESS. Science **322**: 1113-1116.

Lau, O.S., Davies, K.A., Chang, J., Adrian, J., Rowe, M.H., Ballenger, C.E., Bergmann, D.C. (2014). Direct roles of SPEECHLESS in the specification of stomatal self-renewing cells. Science **345**: 1605-1609.

Lawson, T., and Blatt, M.R. (2014). Stomatal size, speed, and responsiveness impact on photosynthesis and water use efficiency. Plant Physiol. **164**: 1556-1570.

Lawson, T., and Matthews, J. (2020). Guard cell metabolism and stomatal function. Annu. Rev. Plant Biol. **71**: 273-302.

Li, J., Nagpal, P., Vitart, V., McMorris, T.C., Chory, J. (1996). A role for brassinosteroids in light-dependent development of Arabidopsis. Science **272**: 398-401.

Li, L., Liu, K.H., and Sheen, J. (2021). Dynamic nutrient signaling networks in plants. Annu. Rev. Cell Dev. Biol. **37**: 341-367.

Lopes, F.L., Formosa-Jordan, P., Malivert, A., Margalha, L., Confraria, A., Feil, R., Lunn, J.E., Jönsson, H., Landrein, B., Baena-González, E. (2024). Sugar signaling modulates SHOOT MERISTEMLESS expression and meristem function in Arabidopsis. Proc. Natl. Acad. Sci. USA **121**: e2408699121.

L**opez-Anido, C.B., Vatén, A., Smoot, N.K., Sharma, N., Guo, V., Gong, Y., Anleu, Gil, M.X., Weimer, A.K., Bergmann, D.C.** (2021). Single-cell resolution of lineage trajectories in the Arabidopsis stomatal lineage and developing leaf. Dev Cell. **56**: 1043-1055.

MacAlister, C.A., Ohashi-Ito, K., and Bergmann, D.C. (2007). Transcription factor control of asymmetric cell divisions that establish the stomatal lineage. Nature **445**: 537-540.

Mair, A., Pedrotti, L., Wurzinger, B., Anrather, D., Simeunovic, A., Weiste, C., Valerio, C., Dietrich, K., Kirchler, T., Nägele, T., et al. (2015). SnRK1-triggered switch of bZIP63 dimerization mediates the low-energy response in plants. Elife **4**: e05828.

Muralidhara, P., Weiste, C., Collani, S., Krischke, M., Kreisz, P., Draken, J., Feil, R., Mair, A., Teige, M., Müller, M.J., et al. (2021). Perturbations in plant energy homeostasis prime lateral root initiation via SnRK1-bZIP63-ARF19 signaling. Proc. Natl. Acad. Sci. USA **118**: e2106961118.

Nadeau, J.A., and Sack, F.D. (2002). Stomatal development in Arabidopsis. Arabidopsis Book **1**: e0066.

Nolan, T.M., Vukašinović, N., Liu, D., Russinova, E., Yin, Y. (2020). Brassinosteroids: multidimensional regulators of plant growth, development, and stress responses. Plant Cell **32**: 295-318.

Park, T.K., Lee, S.H., Kim, S.H., Ko, Y.W., Oh, E., Kim, Y.J., Kim, T.W. (2025). Dual regulation of stomatal development by brassinosteroid in Arabidopsis hypocotyls. J Integr Plant Biol. **67**: 258-275.

Pedrotti, L., Weiste, C., Nägele, T., Wolf, E., Lorenzin, F., Dietrich, K., Mair, A., Weckwerth, W., Teige, M., Baena-González, E., et al. (2018). Snf1-Related Kinase1-controlled C/S1-bZIP signaling activates alternative mitochondrial metabolic pathways to ensure plant survival in extended darkness. Plant Cell **30**: 495-509.

Peng, P., Yan, Z., Zhu, Y., Li, J. (2008). Regulation of the Arabidopsis GSK3-like kinase BRASSINOSTEROID-INSENSITIVE 2 through proteasome-mediated protein degradation. Mol. Plant. **1**: 338-346.

Pierre, M., Traverso, J.A., Boisson, B., Domenichini, S., Bouchez, D., Giglione, C., Meinnel, T. (2007). N-myristoylation regulates the SnRK1 pathway in Arabidopsis. Plant Cell. **19**: 2804-2821.

Pillitteri, L.J., and Torii, K.U. (2012). Mechanisms of stomatal development. Annu. Rev. Plant Biol. **63**: 591-614.

Pillitteri, L.J., Sloan, D.B., Bogenschutz, N.L., Torii, K.U. (2007). Termination of asymmetric cell division and differentiation of stomata. Nature **445**: 501-505.

Qi, X., and Torii, K.U. (2018). Hormonal and environmental signals guiding stomatal development. BMC Biol. **16**: 21.

Ramon, M., Dang, T.V.T., Broeckx, T., Hulsmans, S., Crepin, N., Sheen, J., Rolland,

F. (2019). Default activation and nuclear translocation of the plant cellular energy sensor SnRK1 regulate metabolic stress responses and development. Plant Cell **31**: 1614-1632.

Rasmussen, C.G., Humphries, J.A., and Smith, L.G. (2011). Determination of symmetric and asymmetric division planes in plant cells. Annu. Rev. Plant Biol. **62**: 387-409.

Shi, W., Liu, Y., Zhao, N., Yao, L., Li, J., Fan, M., Zhong, B., Bai, M.Y., Han, C. (2024). Hydrogen peroxide is required for light-induced stomatal opening across different plant species. Nat Commun. **15**: 5081.

Shi, W., Wang, L., Yao, L., Hao, W., Han, C., Fan, M., Wang, W., Bai, M.Y. (2022). Spatially patterned hydrogen peroxide orchestrates stomatal development in Arabidopsis. Nat. Commun. **13**: 5040.

Van Leene, J., Eeckhout, D., Gadeyne, A., Matthijs, C., Han, C., De Winne, N., Persiau, G., Van De Slijke, E., Persyn, F., Mertens, T., et al. (2022). Mapping of the plant SnRK1 kinase signalling network reveals a key regulatory role for the class II T6P synthase-like proteins. Nat. Plants **8**: 1245-1261.

Vukašinović, N., Hsu, C.W., Marconi, M., Li, S., Zachary, C., Shahan, R., Szekley, P., Aardening, Z., Vanhoutte, I., Ma, Q., et al. (2025). Polarity-guided uneven mitotic divisions control brassinosteroid activity in proliferating plant root cells. Cell **188**: 2063-2080.

Vukašinović, N., Wang, Y., Vanhoutte, I., Fendrych, M., Guo, B., Kvasnica, M., Jiroutová, P., Oklestkova, J., Strnad, M., Russinova, E. (2021). Local brassinosteroid biosynthesis enables optimal root growth. Nat. Plants **7**: 619-632.

Wang, H., Han, C., Wang, J.G., Chu, X., Shi, W., Yao, L., Chen, J., Hao, W., Deng, Z., Fan, M., et al. (2022). Regulatory functions of cellular energy sensor SnRK1 for nitrate signalling through NLP7 repression. Nat Plants. **8**: 1094-1107.

Wang, M., Yang, K., Le, J. (2015). Organ-specific effects of brassinosteroids on stomatal production coordinate with the action of Too Many Mouths. J Integr Plant Biol. **57**: 247-255.

Wang, Y., Li, P., Sun, W., Zhang, T. (2024). Plant cell walls: Emerging targets of stomata engineering to improve photosynthesis and water use efficiency. N. Crops **1**: 100021.

Wang, Y., Perez-Sancho, J., Platre, M.P., Callebaut, B., Smokvarska, M., Ferrer, K., Luo, Y., Nolan, T.M., Sato, T., Busch, W., et al. (2023). Plasmodesmata mediate cell-to-cell transport of brassinosteroid hormones. Nat. Chem. Biol. **19**: 1331-1341.

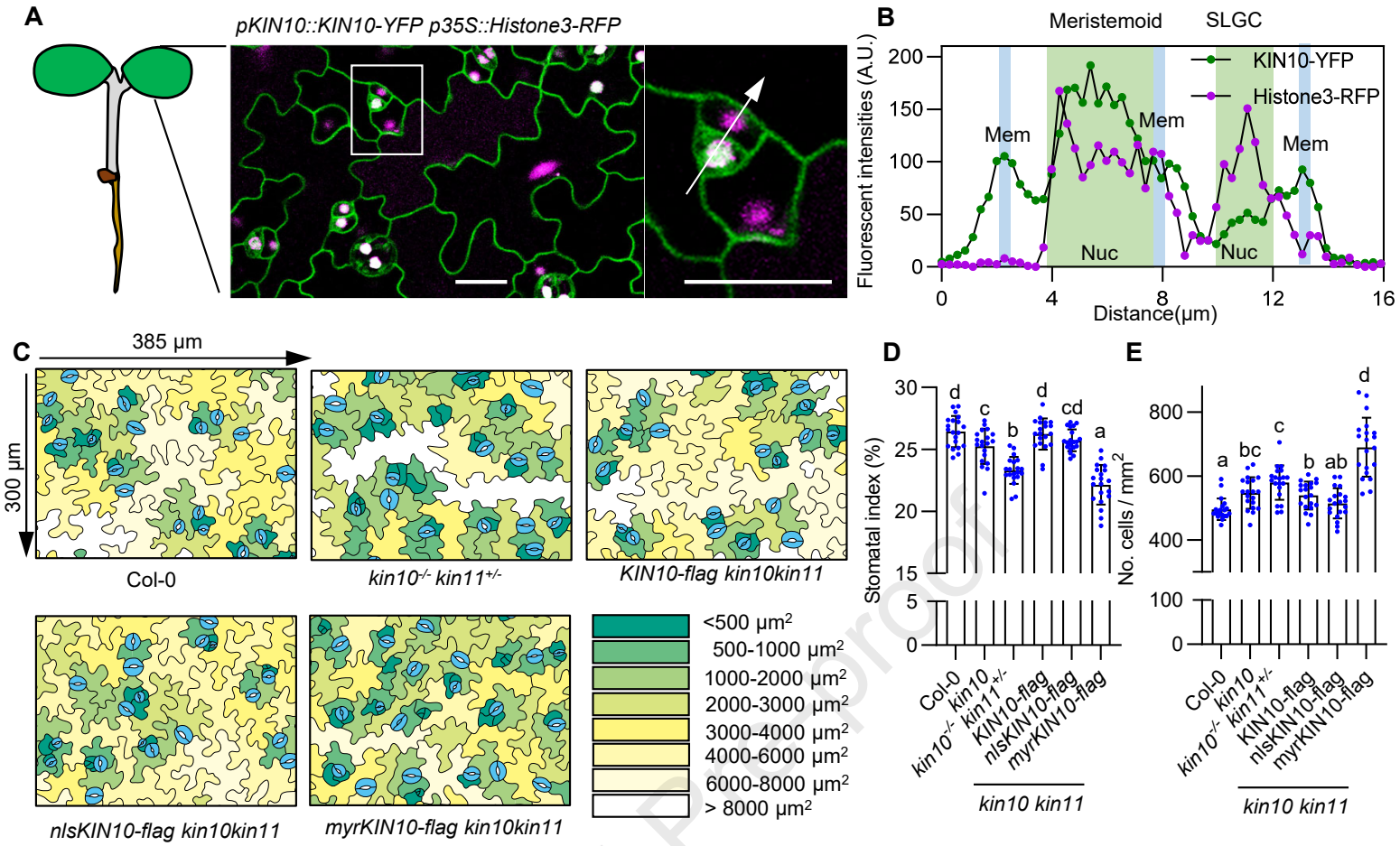
Wang, Z.Y., Nakano, T., Gendron, J., He, J., Chen, M., Vafeados, D., Yang, Y., Fujioka, S., Yoshida, S., Asami, T., et al. (2002). Nuclear-localized BZR1 mediates brassinosteroid-induced growth and feedback suppression of brassinosteroid biosynthesis. Dev. Cell. **2**: 505-513.

Zhang, Y., Xu, T., and Dong, J. (2023). Asymmetric cell division in plant development. J. Integr. Plant Biol. **65**: 343-370.

Journal Pre-proof

Figure 1

Journal Pre-proof



Journal Pre-proof

Figure 2

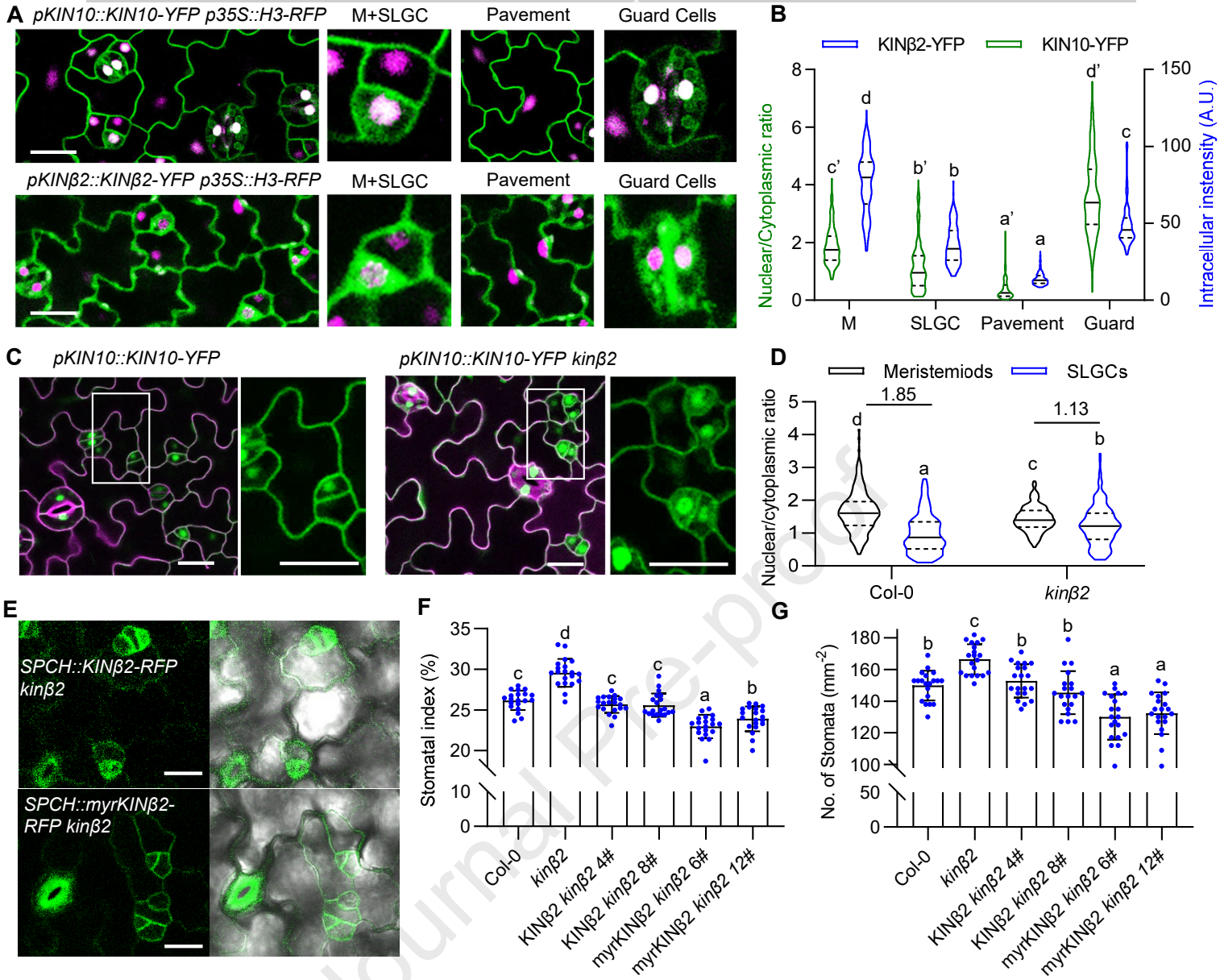
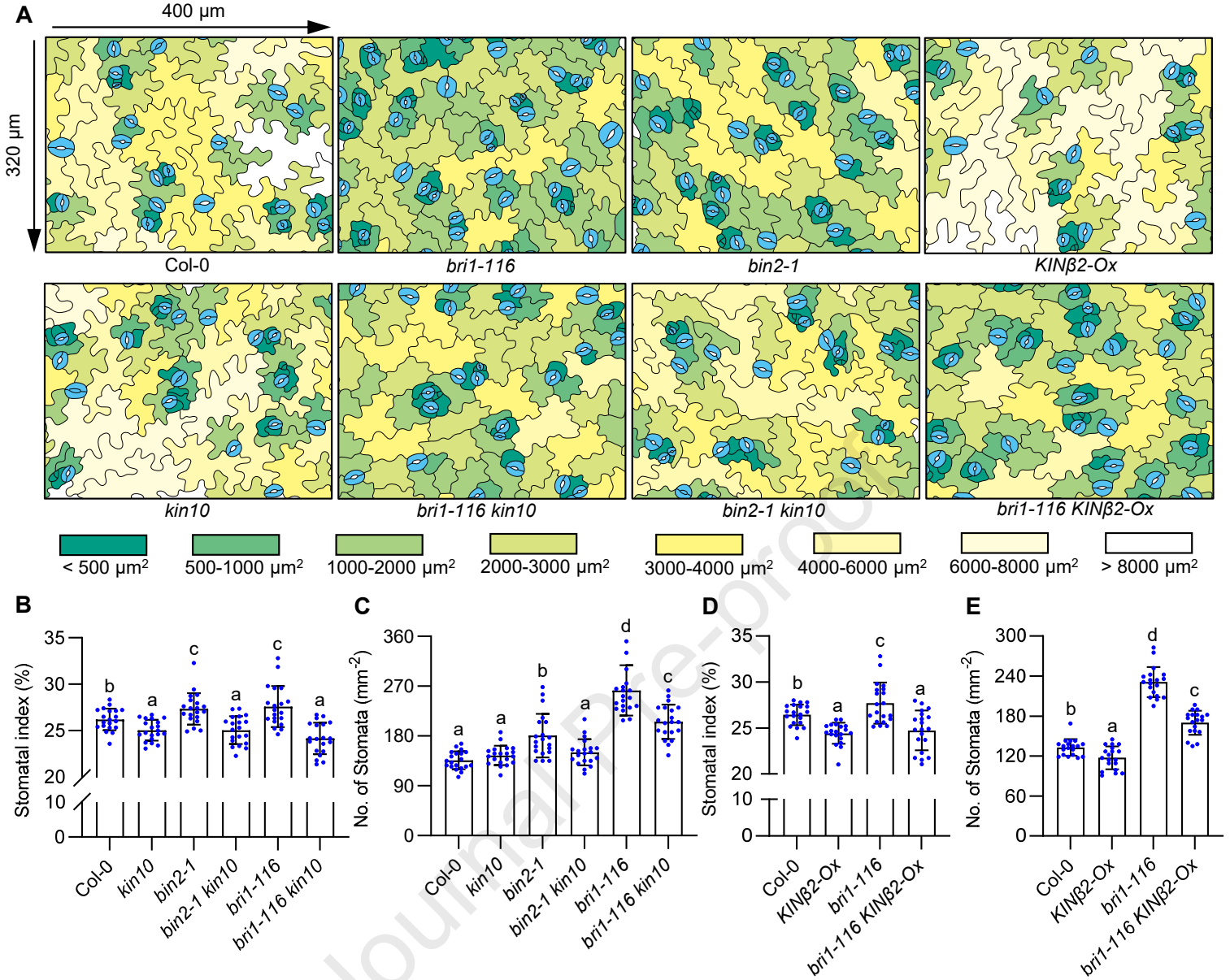


Figure 3

Journal Pre-proof



Journal Pre-proof

Journal Pre-proof

Figure 4

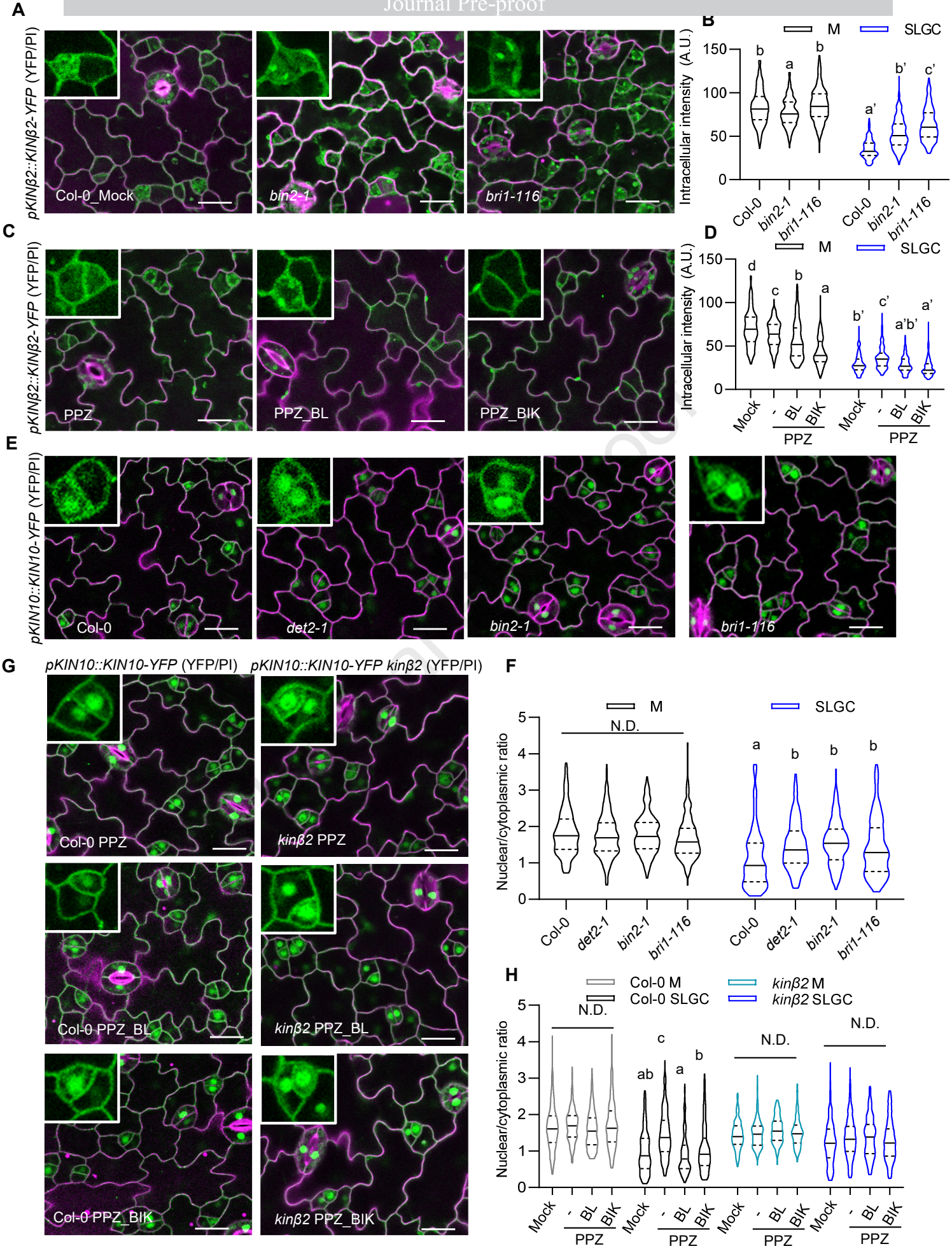


Figure 5

Journal Pre-proof

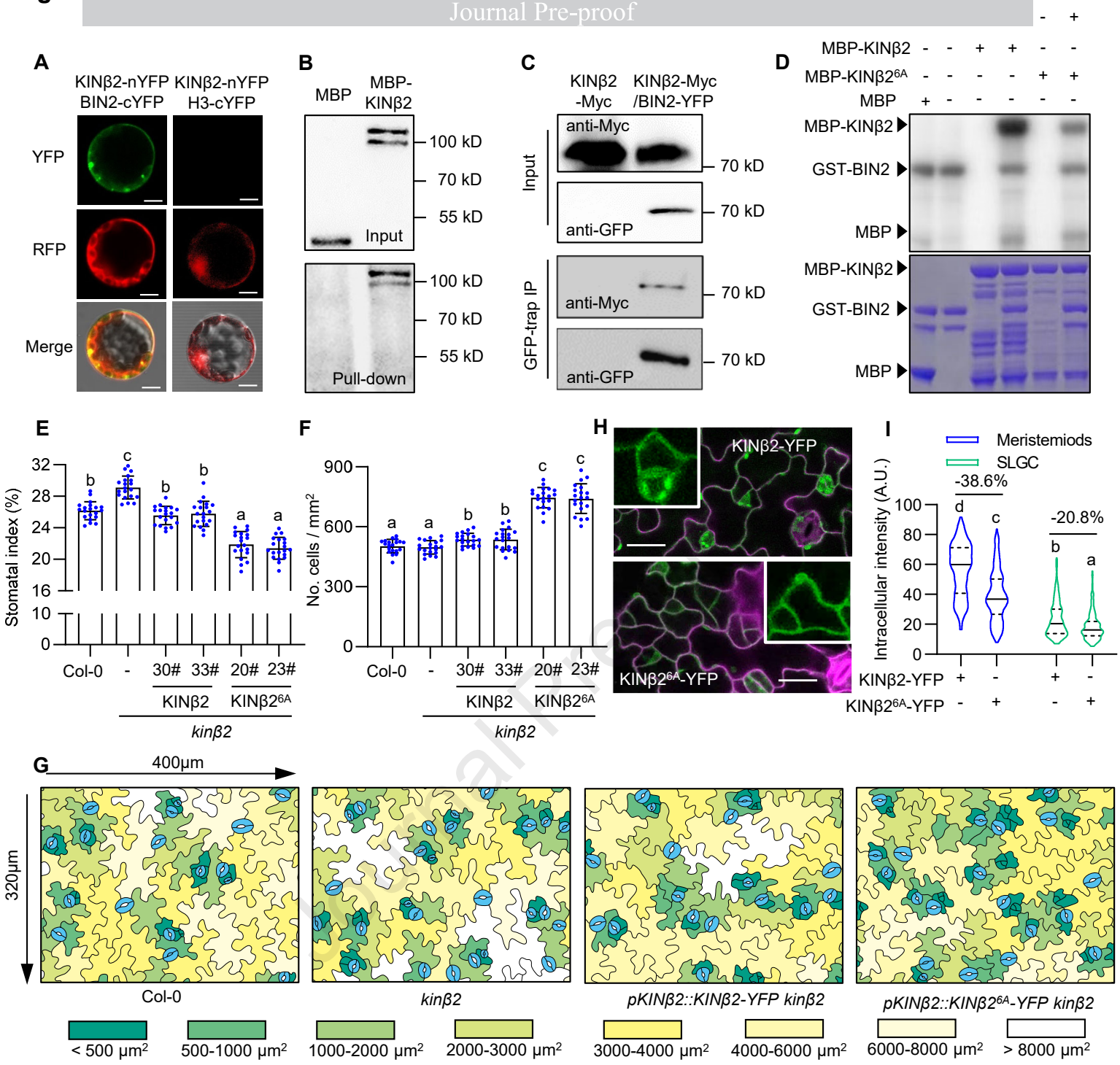


Figure 6

Journal Pre-proof

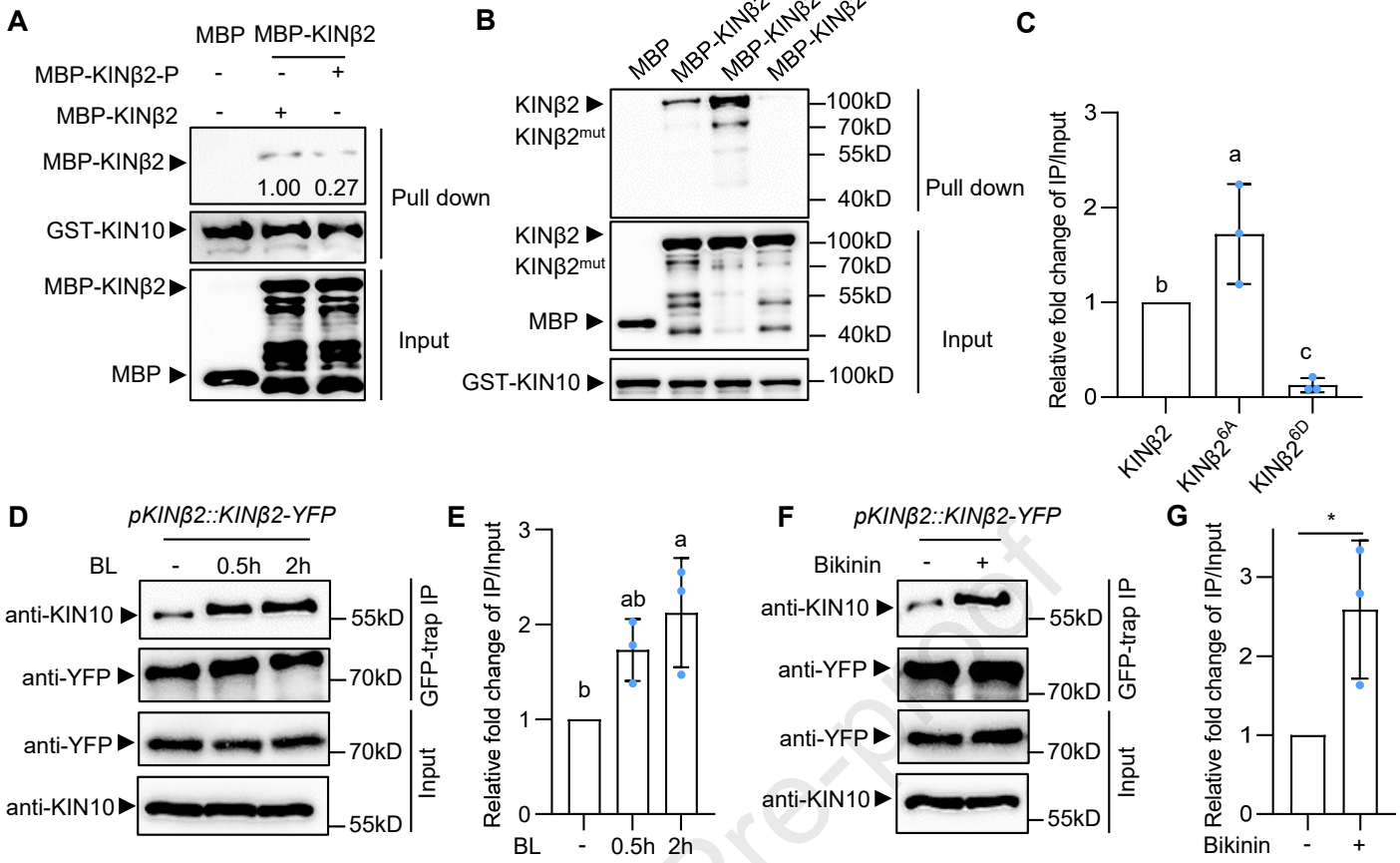
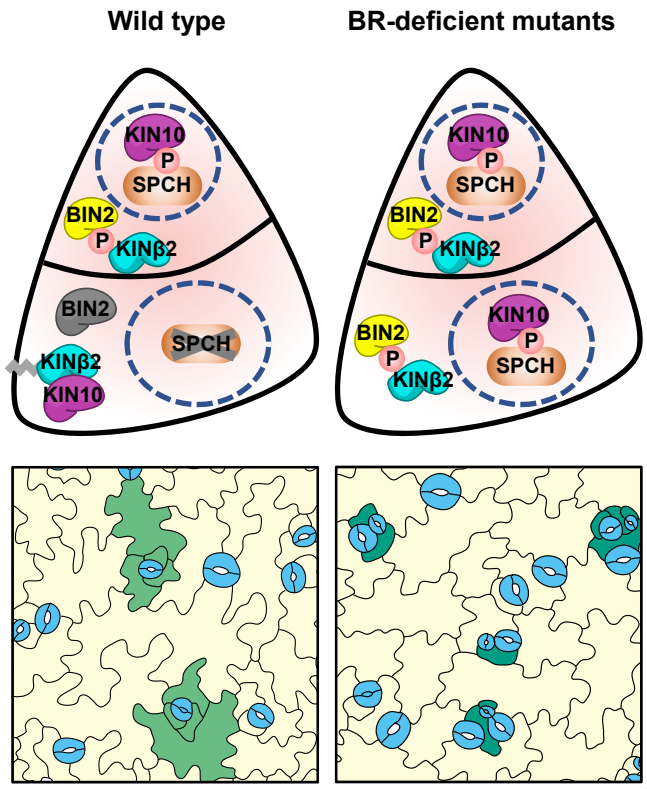


Figure 7



Journal Pre-proof